BJ Structure

Biochem. J. (2012) **446**, 395–404 (Printed in Great Britain) doi:10.1042/BJ20120520

online data

## SUPPLEMENTARY ONLINE DATA

# Crystal structure of the dopamine *N*-acetyltransferase–acetyl CoA complex provides insights into the catalytic mechanism

Kuo-Chang CHENG*, Jhen-Ni LIAO* and Ping-Chiang LYU*†‡[1]

*Institute of Bioinformatics and Structural Biology, National Tsing Hua University, Hsinchu, 30013, Taiwan, †Department of Medical Sciences, National Tsing Hua University, Hsinchu, 30013, Taiwan, and ‡Graduate Institute of Molecular Systems Biomedicine, China Medical University, Taichung, 40402, Taiwan

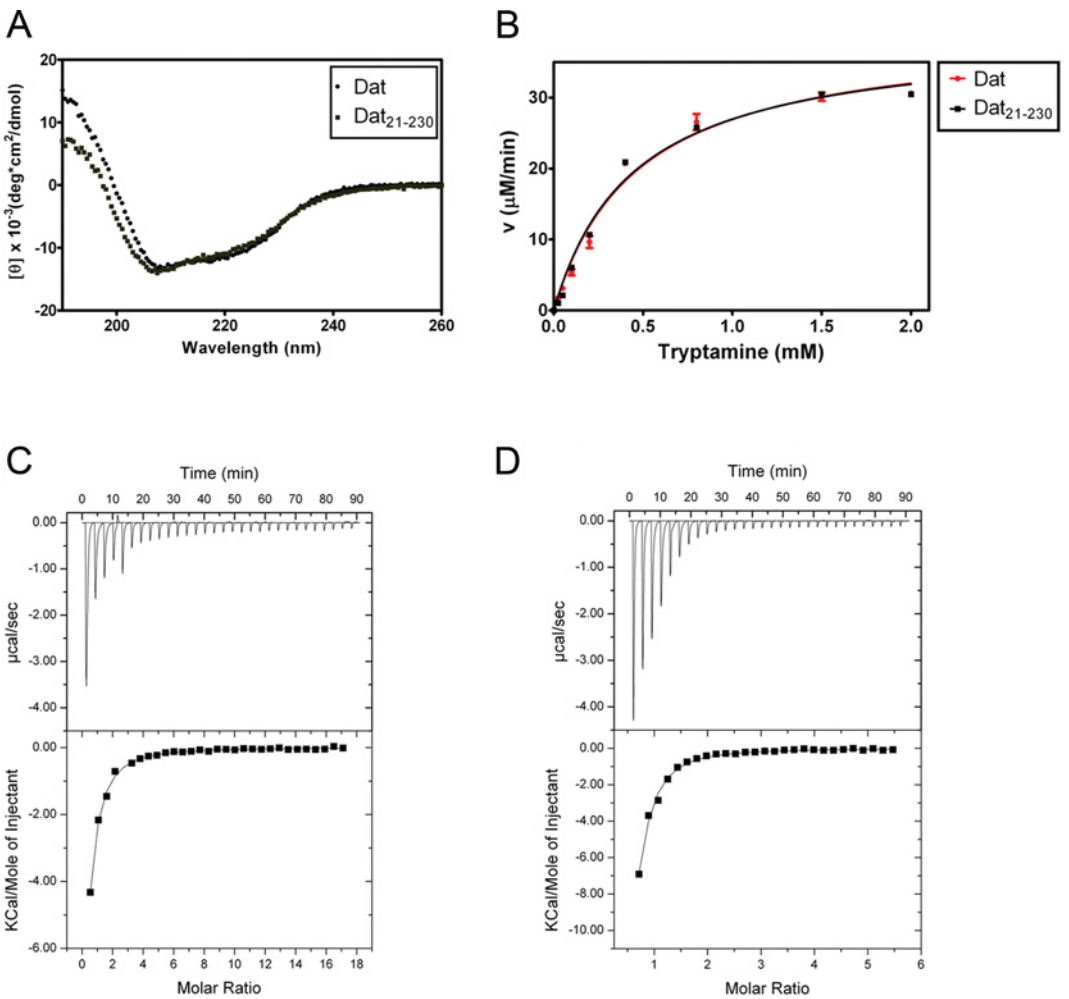


**Figure S1 Comparisons of Dat and $Dat_{21–230}$**

(**A**) CD spectra and (**B**) enzymatic kinetic profiles of Dat and $Dat_{21–230}$. Release of the CoA was used to measure the enzymatic activity. Titrations of dopamine (**C**) and AcCoA (**D**) against $Dat_{21–230}$ were performed. Results are shown for heat change (upper panels) and peak integration (lower panels). The continuous line represents the best fits to a single-site binding model. The binding constants ($K_d$) for dopamine and AcCoA were 12.6 $\mu$M and 2.82 $\mu$M respectively.

The atomic co-ordinates and structural factors have been deposited in the PDB under accession code 3TE4 for the $Dat_{21–230}$–AcCoA complex structure.

[1] To whom correspondence should be addressed (email pclyu@mx.nthu.edu.tw).

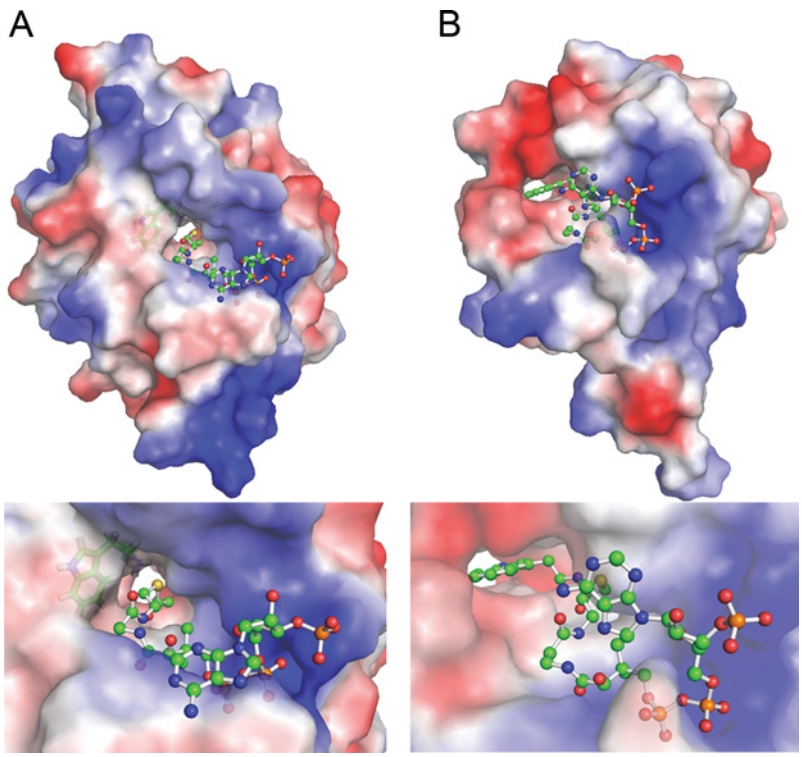


**Figure S2 Substrate- and AcCoA-binding pockets in $Dat_{21–230}$ and in SNAT**

(**A** and **B**) Surface electrostatic potential representations of the active sites in $Dat_{21–230}$ and SNAT respectively. Tryptamine and AcCoA in their respective binding pockets in $Dat_{21–230}$ are shown as stick and ball-and-stick models respectively. In SNAT, the bisubstrate analogue, CoA-S-acetyltryptamine, is shown as ball-and-stick model. The atoms of AcCoA are coloured green (carbon), blue (nitrogen), yellow (sulfur), red (oxygen) and orange (phosphorous). The colour code for the electrostatic potential is blue for positive charges and red for negative charges. The bottom panels are close-ups of the active sites.

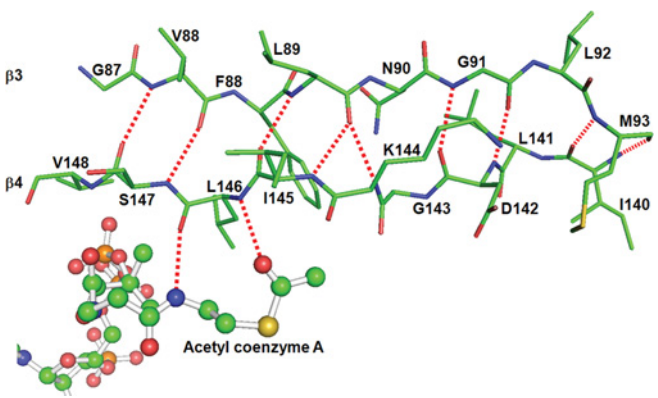


**Figure S3 The $Dat_{21-230}$ $\beta$-bulge**

The residues of $\beta$3 and $\beta$4 are shown as stick models with the $\beta$-bulge formed by $Lys^{144}$ and $Ile^{145}$, which positions their side chains on the same face of the $\beta$-sheet. AcCoA is shown as a ball-and-stick model. The atoms of AcCoA are coloured green (carbon), blue (nitrogen), yellow (sulfur), red (oxygen) and orange (phosphorous). The broken lines indicate hydrogen bonds.

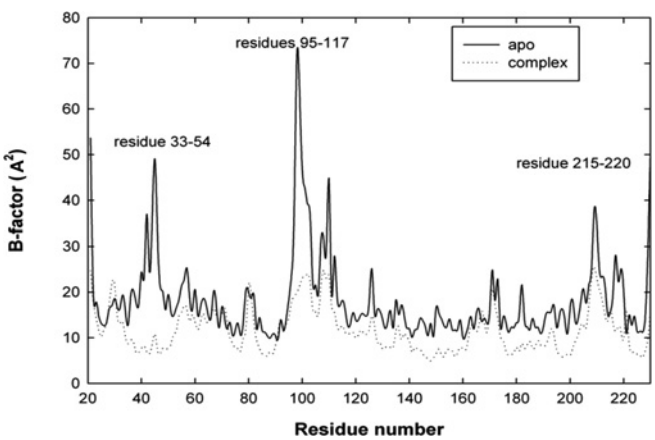


**Figure S4 Temperature factor plots of Dat crystal structures in apo form and complex form**

Plot of main-chain temperature factors for the apo form (continuous line) and complex form (broken line) of Dat crystal structures. In the complex structure, three regions, residues 35–54, 95–117 and 215–220, show significantly lower temperature factors compared with that of the apo form.

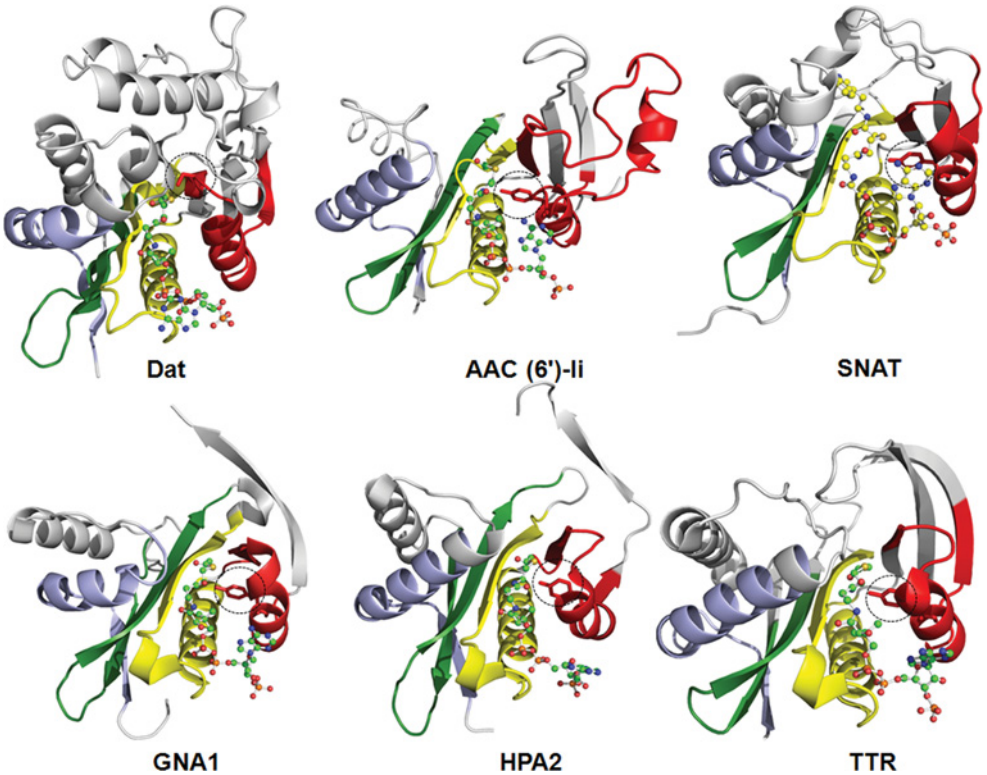


**Figure S5 Structures of $Dat_{21–230}$ and other GCN5 *N*-acetyltransferase domains**

The conserved GNAT motifs C, D, A and B are coloured light blue, green, yellow and red respectively. AcCoA is shown as a ball-and-stick model. The conserved catalytic tyrosine residues (serine in Dat) are shown as red stick models (highlighted in the broken circle). AAC (6′)-Ii, aminoglycoside 6′-*N*-acetyltransferase type Ii, *Enterococcus faecium*; GNA1, glucosamine-6-phosphate *N*-acetyltransferase 1, *Saccharomyces cerevisiae*; HPA2, histone acetyltransferase, *Saccharomyces cerevisiae*; SNAT, serotonin *N*-acetyltransferase, *Ovis aries*; TTR, tabtoxin-resistance protein, *Pseudomonas syringae*.

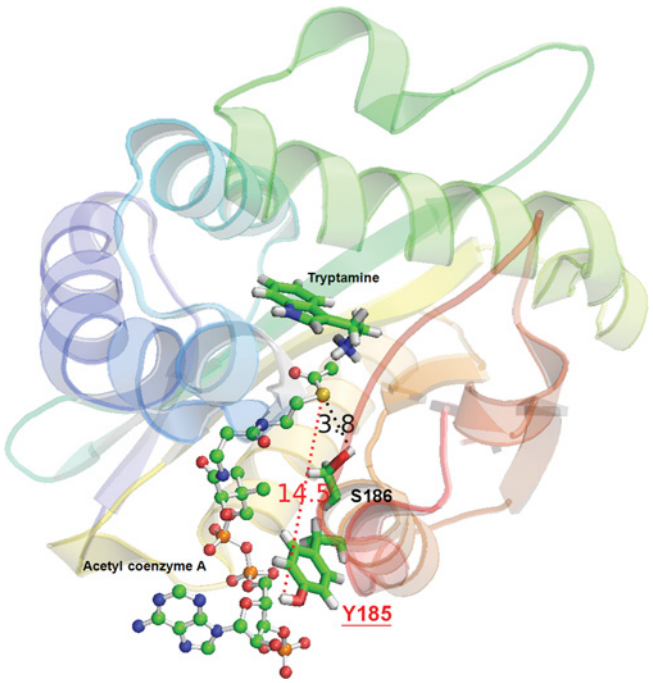


**Figure S6 Structure of $Dat_{21–230}$–AcCoA complex with a docked tryptamine: spatial relationships between potential residues and AcCoA at the active site**

The Dat sequence contains a $Tyr^{185}$ residue just before $Ser^{186}$. The residues $Tyr^{185}$ (red) and $Ser^{186}$ (black) are represented as stick models. The broken lines identify distance between the AcCoA sulfur atom and target residues. The numbers represent distance separations between various atoms in angstroms. Tryptamine is shown as a stick model and AcCoA is shown as a ball-and-stick model.

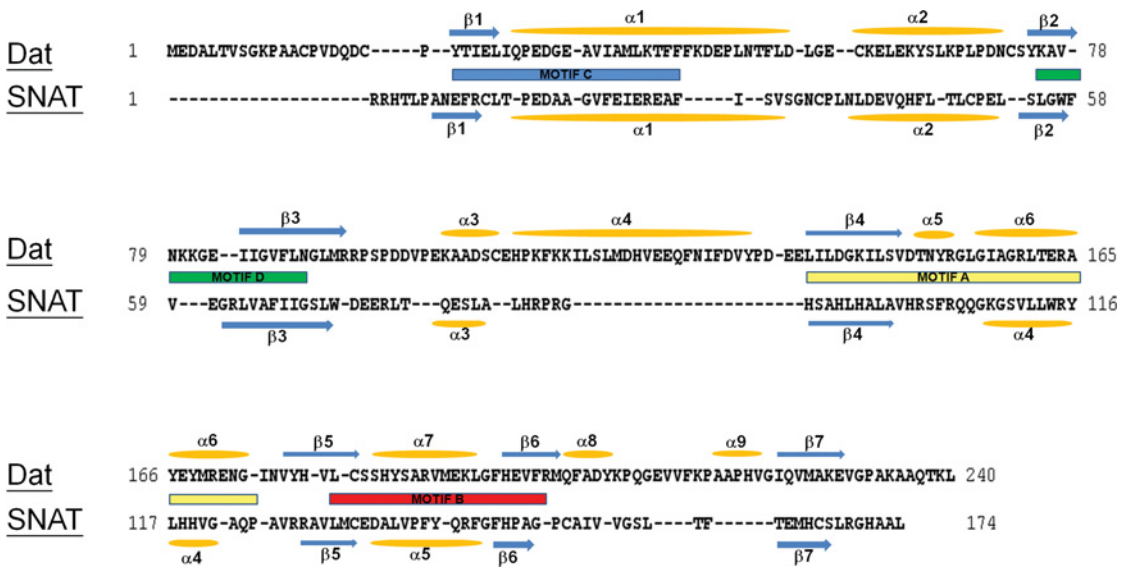


**Figure S7 Structure-based sequence alignment of Dat and *O. aries* SNAT**

To structurally align the sequences, first their three-dimensional structures were manually aligned with gaps introduced as needed. Then, the sequences of the common secondary structural elements were manually aligned with the positions of those in SNAT adjusted so that they were aligned with the corresponding secondary structures in $Dat_{21–230}$. The secondary structure elements in Dat and SNAT are indicated above and below the sequences respectively. The conserved motifs C, D, A and B are shown as boxes coloured cyan, green, yellow and red respectively.

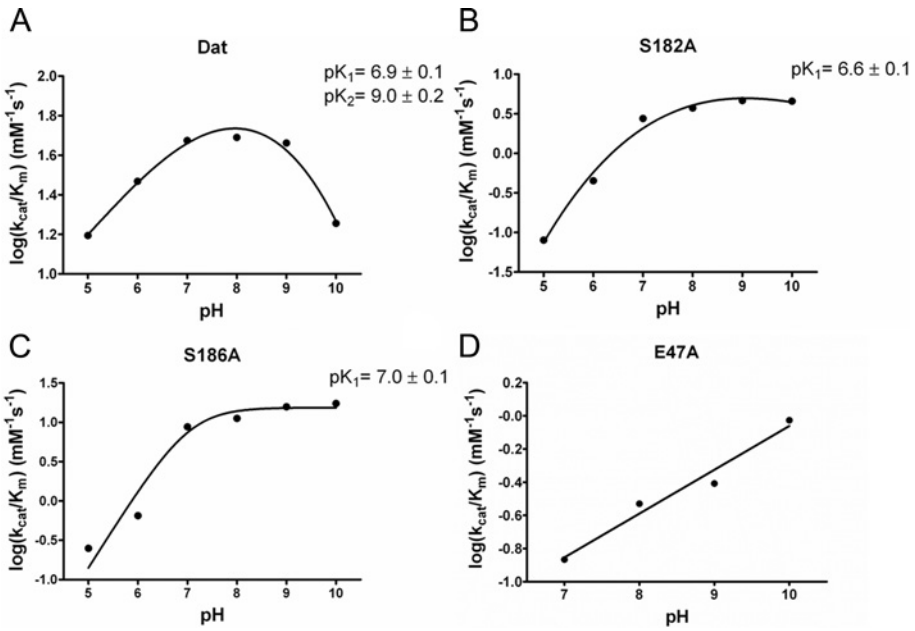


**Figure S8 The pH profiles of log($k_{cat}/K_m$) for wild-type Dat, S182A, S186A and E47A**

The pH-dependence of log($k_{cat}/K_m$) observed for Dat (**A**) are shown with curve fits obtained by non-linear least-squares regression. The p$K_a$ values are given on the graphs. p$K_1$ (6.9±0.1) refers to the acidic limb of the profile, and p$K_2$ (9.0±0.2) represents the basic limb. pH values compared with log($k_{cat}/K_m$) profiles of S182A (**B**) and S186A(**C**) indicate a ionizable residue which is active only in the deprotonated form involved in catalysis with a p$K_a$ of approximately 6.9. The pH profile for the E47A mutant (**D**) was fitted to a line with a slope of 0.3.

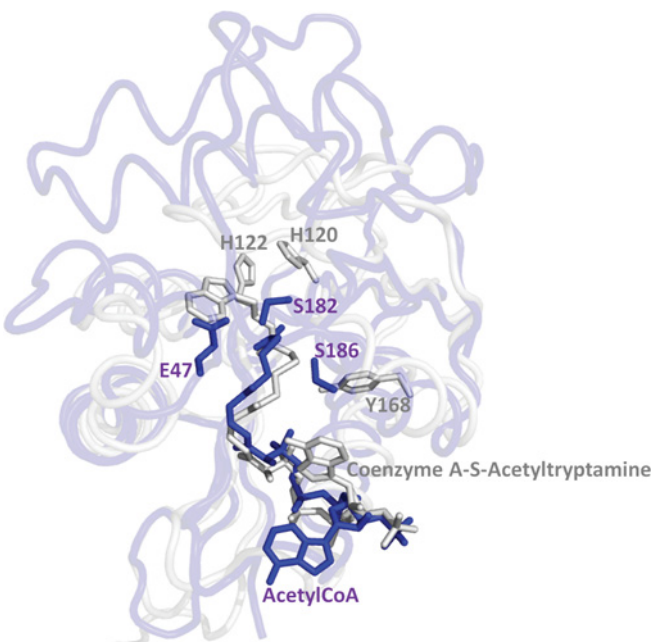


**Figure S9 Comparison of the catalytic triads of AANATs from *D. melanogaster* and *O. aries***

The structural superimposition of Dat (blue) and SNAT (grey). The ligands and catalytic residues for Dat and SNAT are labelled and shown in stick representation in blue and grey respectively. The two structures share a very similar structural fold despite low sequence identity (12 %), with an RMSD value of 1.89 Å.

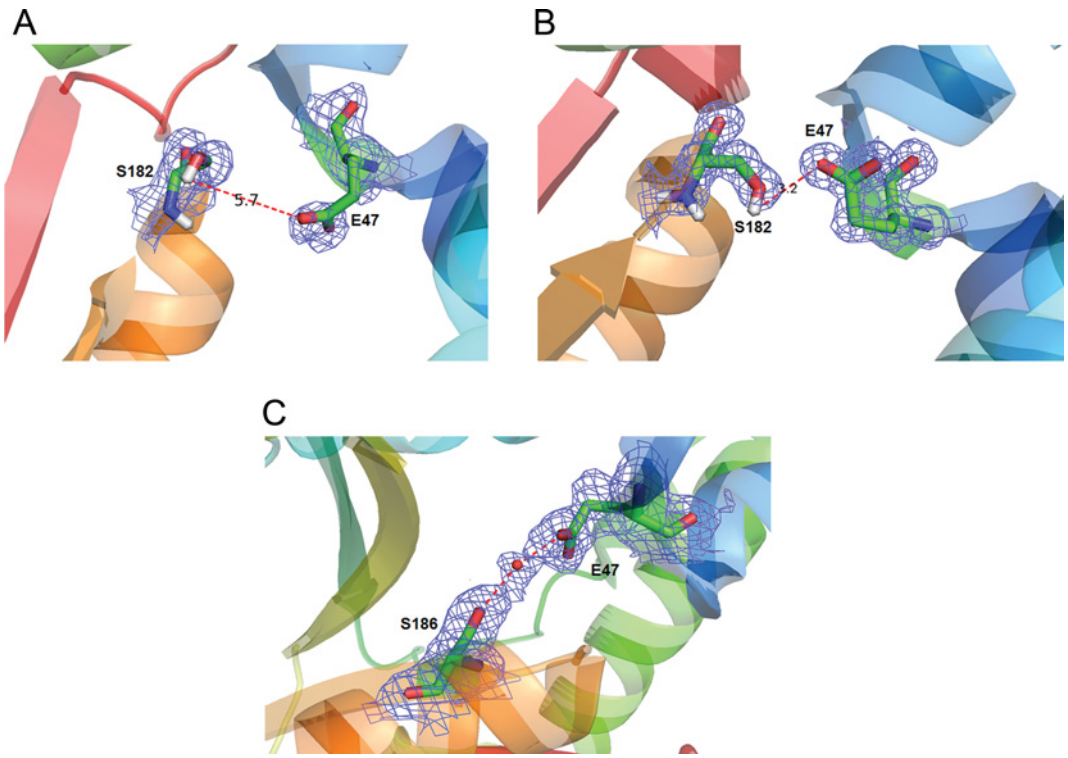


**Figure S10 Comparison of the catalytic triad residues of Dat in apo form and complex form**

The catalytic triad residues Glu$^{47}$ and Ser$^{182}$ are represented as stick models in the apo form (**A**) and complex form (**B**) of the Dat structure. The broken lines identify the distance between the catalytic residues. The numbers represent distance separations between various atoms in angstroms. (**C**) The catalytic triad residues Glu$^{47}$ and Ser$^{186}$ form a hydrogen bond network with each other by a proton-conducting water molecule (shown as a red ball). The density, shown as a blue mesh, is a $2F_o - F_c$ map, contoured at 1.1 $\sigma$. Note that, by comparing the Dat structure between apo form and complex form, two crystallographic facts could implicate the catalytic role of Glu$^{47}$: (i) the distance between the Glu$^{47}$ carboxylate anion and Ser$^{182}$ hydroxy group decreased after formation of the Dat–AcCoA complex structure, which enabled Glu$^{47}$ to abstract a proton from the hydroxy group of Ser$^{182}$. Moreover, the carboxylate of Glu$^{47}$ forms a hydrogen bond to a proton-conducting water molecule. This water molecule is co-ordinated by hydrogen bonding and is 2.8 Å away from the hydroxy oxygen of Ser$^{186}$ in an appropriate position to transfer a proton (crystallographic and refinement statistics of the apo form structure are not shown. K.-C. Cheng and P.-C. Lyu, unpublished work).

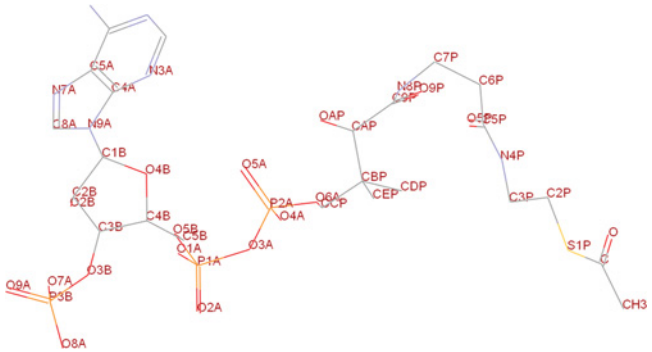


**Figure S11 AcCoA with the atoms labelled as in Table S1**

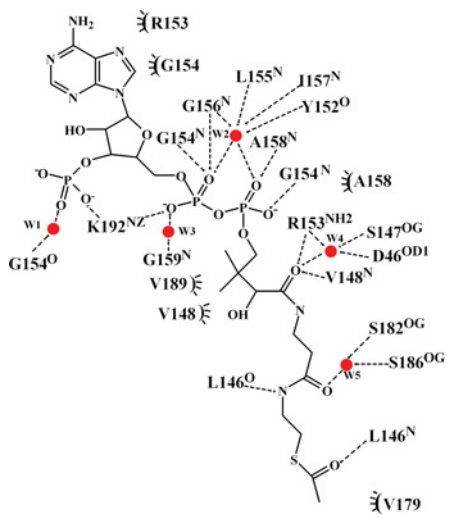


**Figure S12 Schematic diagram of the AcCoA–protein contacts**

**Table S1 Detailed protein–cofactor contacts**

The numbers represent distance separations between cofactor atoms and protein residue atoms in angstroms. See Figures S11 and S12 for more details.

(i) AcCoA salt bridge

| Atom | Salt bridge |
|---|---|
| O8A | $Lys^{192}$ NZ 2.7 |
| O2A | $Lys^{192}$ NZ 2.7 |

(ii) AcCoA hydrogen bonds

| Atom | Hydrogen bond | Water-mediated hydrogen bond |
|---|---|---|
| O7A | W1 2.7 | $Gly^{154}$ O 2.9 |
| O1A | $Gly^{154}$ N 3.3 | – |
| | $Gly^{156}$ N 2.8 | – |
| | W2 3.4 | $Gly^{156}$ N 3.1 |
| | W2 3.4 | $Leu^{155}$ N 2.8 |
| | W2 3.4 | $Ile^{157}$ N 2.9 |
| | W2 3.4 | $Tyr^{152}$ O 2.7 |
| O2A | W3 2.7 | $Gly^{159}$ N 2.8 |
| O4A | $Ala^{158}$ N 2.8 | – |
| | W2 2.7 | $Gly^{156}$ N 3.1 |
| | W2 2.7 | $Leu^{155}$ N 2.8 |
| | W2 2.7 | $Ile^{157}$ N 2.9 |
| | W2 2.7 | $Tyr^{152}$ O 2.7 |
| O5A | $Gly^{154}$ N 2.9 | – |
| O9P | $Arg^{153}$ NH2 3.3 | – |
| | $Val^{148}$ N 3.1 | – |
| | W4 2.9 | $Arg^{153}$ NH2 3.2 |
| | W4 2.9 | $Ser^{147}$ OG 2.7 |
| | W4 2.9 | $Asp^{46}$ OD1 2.8 |
| O5P | W5 2.9 | $Ser^{182}$ OG 2.8 |
| | W5 2.9 | $Ser^{186}$ OG 2.7 |
| N4P | $Leu^{146}$ O 2.9 | |
| O | $Leu^{146}$ N 3.0 | |

(iii) AcCoA van der Waals interactions

| Atom | Van der Waals interaction |
|---|---|
| C2A | $Arg^{153}$ CB 3.5 |
| | $Arg^{153}$ CG 4.3 |
| C5A | $Gly^{154}$ CA 3.8 |
| | $Arg^{153}$ C 4.0 |
| C6A | $Arg^{153}$ CB 3.8 |
| | $Arg^{153}$ CA 4.4 |
| C8A | $Gly^{154}$ CA 3.7 |
| C5B | $Val^{189}$ CG2 3.7 |
| CCP | $Val^{189}$ CG2 4.2 |
| | $Ala^{158}$ CB 3.8 |
| CDP | $Leu^{146}$ CG 3.6 |
| | $Val^{148}$ CG2 3.8 |
| CEP | $Val^{189}$ CG2 4.4 |
| C9P | $Arg^{153}$ CZ 3.6 |
| CH3 | $Val^{179}$ CG1 3.8 |

Received 26 March 2012/11 June 2012; accepted 21 June 2012
Published as BJ Immediate Publication 21 June 2012, doi:10.1042/BJ20120520